Hindawi
Journal of Nanomaterials
Volume 2020, Article ID 4917946, 9 pages
https://doi.org/10.1155/2020/4917946

Research Article

Analysis of Electrical Characteristics of Pd/*n*-Nanocarbon/*p*-Si Heterojunction Diodes: By *C-V-f* and *G/w-V-f*

Abdelrahman Zkria[1,2], **Eslam Abubakr**[1,3], **Phongsaphak Sittimart**[1] and **Tsuyoshi Yoshitake**[1]

[1]*Department of Applied Science for Electronics and Materials, Kyushu University, Kasuga, Fukuoka 816-8580, Japan*
[2]*Department of Physics, Faculty of Science, Aswan University, Aswan 81528, Egypt*
[3]*Department of Electrical Engineering, Faculty of Engineering, Aswan University, Aswan 81542, Egypt*

Correspondence should be addressed to Abdelrahman Zkria; abdelrahman_zkria@kyudai.jp

Received 27 February 2020; Revised 13 May 2020; Accepted 27 June 2020; Published 17 July 2020

Academic Editor: David Cornu

Copyright © 2020 Abdelrahman Zkria et al. This is an open access article distributed under the Creative Commons Attribution License, which permits unrestricted use, distribution, and reproduction in any medium, provided the original work is properly cited.

Diamond films are candidate for a wide range of applications, due to their wide band gap, high thermal conductivity, and chemical stability. In this report, diamond-based heterojunction diodes (HJDs) were fabricated by growing *n*-type nanocarbon composite in the form of nitrogen-doped ultrananocrystalline diamond/amorphous carbon (UNCD/a-C:H:N) films onto *p*-type Si substrates. X-ray photoemission and the Fourier transform infrared spectroscopies were employed to examine the contribution of nitrogen atoms from the gas phase into the deposited films. The results indicate the incorporation of nitrogen atoms into the grain boundaries of UNCD/a-C:H film by replacing hydrogen atoms. The capacitance- (*C-V-f*), conductance- (*G/ω-V-f*), and series resistance-voltage characteristics of the fabricated Pd/*n*-(UNCD/a-C:H:N)/*p*-Si HJDs were studied in the frequency range of 40 kHz-2 MHz. The existence of interface states (N_{ss}) and series resistance (R_s) were attributed to the interruption of the periodic lattice structure at the surface of the fabricated junction as well as the defects on the (UNCD/a-C:H:N)/Si interface. By increasing the frequency (≥500 kHz), the N_{ss} reveals an almost frequency-independent behavior, which indicates that the charges at the interface states cannot follow ac signal at higher frequency. The obtained results demonstrated that the UNCD/a-C:H:N is a promising *n*-type semiconductor for diamond-based heterostructure diodes.

1. Introduction

Carbon is a unique chemical element because it morphs into up to 32 allotropes, such as graphite and diamond, which represent sp^2- and sp^3-orbital hybridization, respectively. Recently, diamond has triggered many research activities for new-type optoelectronics and high temperature-high frequency devices [1, 2]. However, the formation of *n*-type diamond by nitrogen doping has always been one of the biggest struggles in diamond field, due to the deep nitrogen donor level (1.7 eV) as well as the nitrogen-associated defects that influence the carrier transport [3]. In contrast, ultrananocrystalline diamond (UNCD) can be doped with nitrogen with low activation energy wherein the *n*-type conduction primarily related to the grain boundary network [4].

It was found that nitrogen dopants create additional electric conduction paths in UNCD films [5]. Ikeda et al. [6] correlated the enhancement of electrical conductivity of nitrogen-doped UNCD films to the enlargement of ordering and fraction of sp^2-carbon at the grain boundary. Mertens et al. [7] have studied the electrical conductivity of nitrogen-doped UNCD films. Their results suggest that the *n*-type conduction depends on the structure and volume of the grain boundary.

Although UNCD/a-C:H:N films are mainly grown by the chemical vapor deposition (CVD) method [8, 9], the authors have previously grown them by coaxial arc plasma (CAPD) [10] and pulsed laser deposition (PLD) [11]. In our previous works, we studied *n*-type (UNCD/a-C:H:N)/*p*-type Si HJDs by the CAPD method [12–14]. The fabricated diode

exhibited a rectifying action with 10^4 rectification ratio in the bias range ±1 V. Additionally, the Pd/*n*-(UNCD/a-C:H:N)/*p*-Si photodiodes showed a capability of deep ultraviolet light detection under the 254 nm monochromatic light [14, 15]. In addition, we investigated the origin of dark current in Pd/*n*-(UNCD/a-C:H:N)/*p*-Si HJDs based on an established comprehensive computer device model [16].

In prior reports, we characterized the Pd/*n*-(UNCD/a-C:H:N)/*p*-Si HJDs by employing I-V measurements at room and low temperatures. However, the effects of interface state density (N_{ss}) and series resistance (R_s) on their electrical characteristics were not investigated. Practically, the N_{ss} and R_s can be studied by the low-high frequency capacitance (C_{LF}-C_{HF}), Hill-Coleman, and Nicollian and Brews techniques [17, 18]. Many researchers have proposed the frequency-dependent *C-V* and *G*/*ω*-*V* method as being effective to determine the electrical characteristics of HJDs composed of various materials including diamond [19], graphene [20], ZnGaSe [21], and ZnGaTe [22]. Although *C-V* and *G*/*ω*-*V* measurements in ideal diodes are frequency independent [23], N_{ss} and R_s significantly influence the device characteristics and cause considerable deviation from ideality [24]. The aim of this study is to investigate the influence of R_s and N_{ss} on the electrical characteristics of Pd/*n*-(UNCD/a-C:H:N)/*p*-Si HJDs. Therefore, frequency-dependent *C-V* and *G*/*ω*-*V* measurements were performed over the wide-range frequency of 40 kHz-2 MHz at room temperature.

2. Experiments

2.1. Film Deposition and Structural Investigations. 400 nm thin-nitrogen-doped UNCD/a-C:H:N films (undoped films for comparison) were grown in nitrogen and hydrogen gases atmosphere of 53.3 Pa at a substrate temperature of 550°C by coaxial arc plasma deposition (CAPD) using a pure graphite target. An arc plasma gun connected with (720 μF) capacitor was conducted at 5 Hz repetition rate. In order to investigate nitrogen atoms incorporation and estimate their contents into the deposited films, X-ray photoemission spectroscopy (Mg Kα line, hν = 1253.6 eV) has been employed. In this study, the nitrogen content of the film deposited at a nitrogen/hydrogen ratio ($I_{N/H}$) of 0.25 was estimated to be 3 at.%, by similar method in our previous report [25]. In addition, Fourier transform infrared (FTIR) spectra were recorded in the middle of the infrared range from 400 to 4000 cm^{-1} for deposited films, and the CH band spectra were deconvoluted into the Gaussian peaks.

2.2. Fabrication and Characterization of the Heterojunction Diodes. In order to fabricate the heterojunction diodes, *n*-type (UNCD/a-C:H:N) films were grown onto (111) *p*-type (boron-doped) single crystal silicon (Si) by the CAPD method. *p*-Type Si substrates, having a thickness of 200 μm and 1.3-3 Ω cm resistivity, were treated by (CH3) 2CO (acetone), CH3OH (methanol), and distilled water for 5 min, sequentially. For ohmic contact, palladium (Pd) electrodes were sputtered from pure Pd target (99.99%) using a radio-frequency magnetron sputtering apparatus. Pd electrodes with a thickness of 120 nm were deposited on the back side (*p*-Si), and with a square mask with a device area of 0.1 cm^2 on the front side (film) of the fabricated diodes. The sputtering deposition was operated at a pressure of 2.66×10^{-1} Pa in argon atmosphere with a flow rate of 15 sccm. *C-V* and *G*/*ω*-*V* measurements were performed in the frequency range of 40 kHz-2 MHz with an applied ac bias of 50 mV by using a precision LCR meter (Agilent E4980A). By analyzing the *C-V-f* and *G*/*ω*-*V-f* measurements, R_s and N_{ss} were extracted using the Nicollian-Brews and Hill-Coleman methods, respectively.

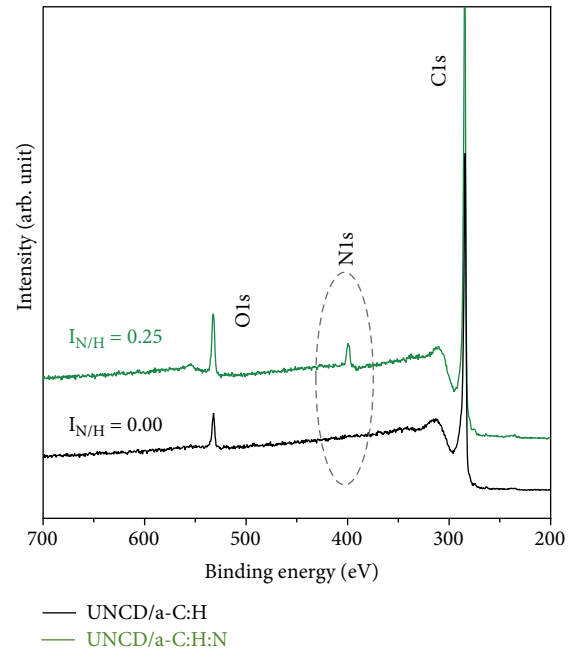

Figure 1: X-ray photoemission spectra of undoped and nitrogen-doped UNCD/a-C:H films. N1s peak confirms the incorporation of nitrogen atoms into the film.

3. Results and Discussion

3.1. Structural Investigations: By XPS and FTIR. XPS is a powerful tool to estimate the amount ratio between sp^2 and sp^3 bonds in their coexistence materials. Figure 1 depicts wide-scan XPS spectra of undoped and nitrogen-doped UNCD/a-C:H films with sharp C1s peaks, in addition to O1s peaks originated from the film surface. The nitrogen-doped UNCD/a-C:H:N film revealed an extra peak at 409 eV referring to N1s peak [26], which confirms the incorporation of nitrogen atoms into the UNCD/a-C:H film from the hydrogen/nitrogen ambient gases inside the CAPD chamber. To investigate the chemical structure in more detail, C1s photoemission spectrum was recorded using synchrotron radiation.

In Figure 2(a), the XPS C1s core spectra of the undoped and nitrogen-doped UNCD/a-C:H films are shown. The spectra depict slightly broader peak of the nitrogen-doped film compared with that of the undoped UNCD/a-C:H film. This observation refers to the formation of the peaks at 284.4, 285.4, 286.7, and 287.6 eV, which are assigned to sp^2-C bonds, sp^3-C bonds, Cn bonds, and C=O bonds, respectively

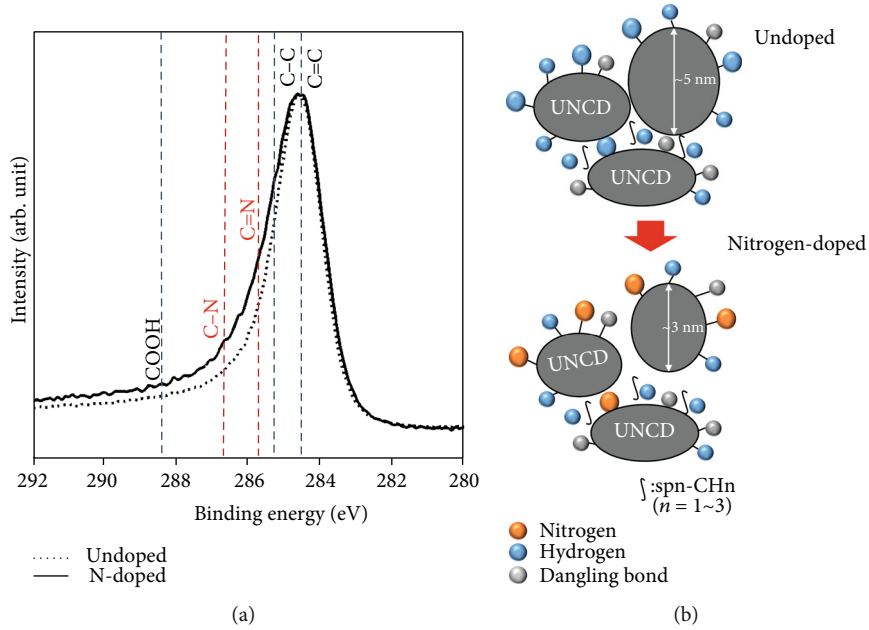

Figure 2: (a) C1s peak of XPS spectra for undoped (solid line) and nitrogen-doped (dashed line) UNCD/a-C:H films. (b) Illustration of N atoms incorporated into GBs (a-C-H) by replacing H atoms.

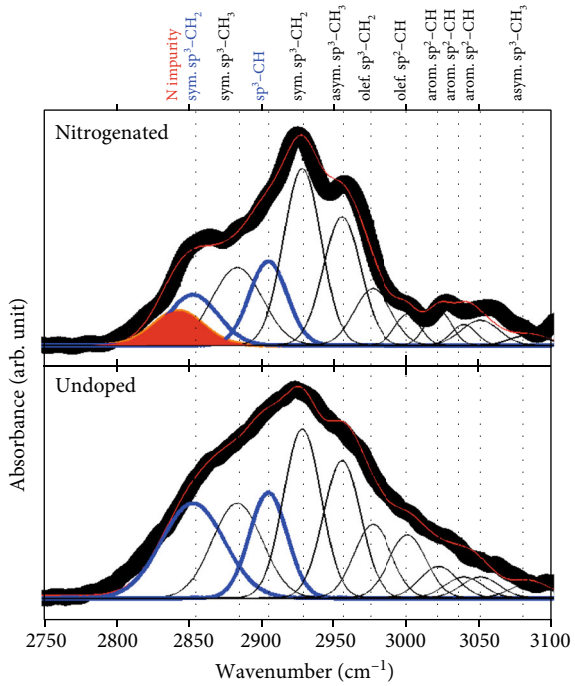

Figure 3: FTIR spectra of undoped and nitrogen-doped UNCD/a-C:H films grown by CAPD method, decomposed into the Gaussian peaks.

[27]. Figure 2(b) illustrates the suggested mechanism of nitrogen incorporation into grain boundaries by replacing hydrogen atoms.

Figure 3 shows the FTIR spectra of undoped and nitrogen-doped UNCD/a-C:H films in the range of 2750-3100 cm^{-1}, which contain different superpositioned CH_n ($n = 1,2,3$) vibration peaks. The spectra were deconvoluted for Gaussian peaks based on our earlier study [28], and the positions of separated peaks are summarized in Table 1. Compared to the undoped film, the FTIR spectrum of N-doped UNCD/a-C:H divulged two extra peaks at 2844 and 3049 cm^{-1}, attributable to nitrogen impurities [29] and aromatic nucleus CH stretching vibration [30], respectively. In addition, the sp^3-CH and sp^3-CH_2 peaks, which might originate from hydrogen atoms, are clearly weakened, which implies that hydrogen atoms at the grain boundaries are replaced by nitrogen atoms. These results indicate that the nitrogen doping not only forms carbon-nitrogen bonds (C–N and C=N) but also expedites the sp^2-CH_n, which is

Table 1: Summary of the peak positions in FTIR spectra and assigned vibration mode of undoped and nitrogen-doped UNCD/a-C:H films.

Wavenumber (cm^{-1})	Vibration mode
2844	N impurities
2854	sym. sp^3-CH_2
2884	sym. sp^3-CH_3
2905	sp^3-CH
2928	sym. sp^3-CH_2
2955	Asym. sp^3-CH_3
2976	Olefinic sp^2-CH_2
3000	Olefinic sp^2-CH
3021	Aromatic sp^2-CH
3038	Aromatic sp^2-CH
3049	Aromatic sp^2-CH
3082	Aromatic sp^2-CH_3

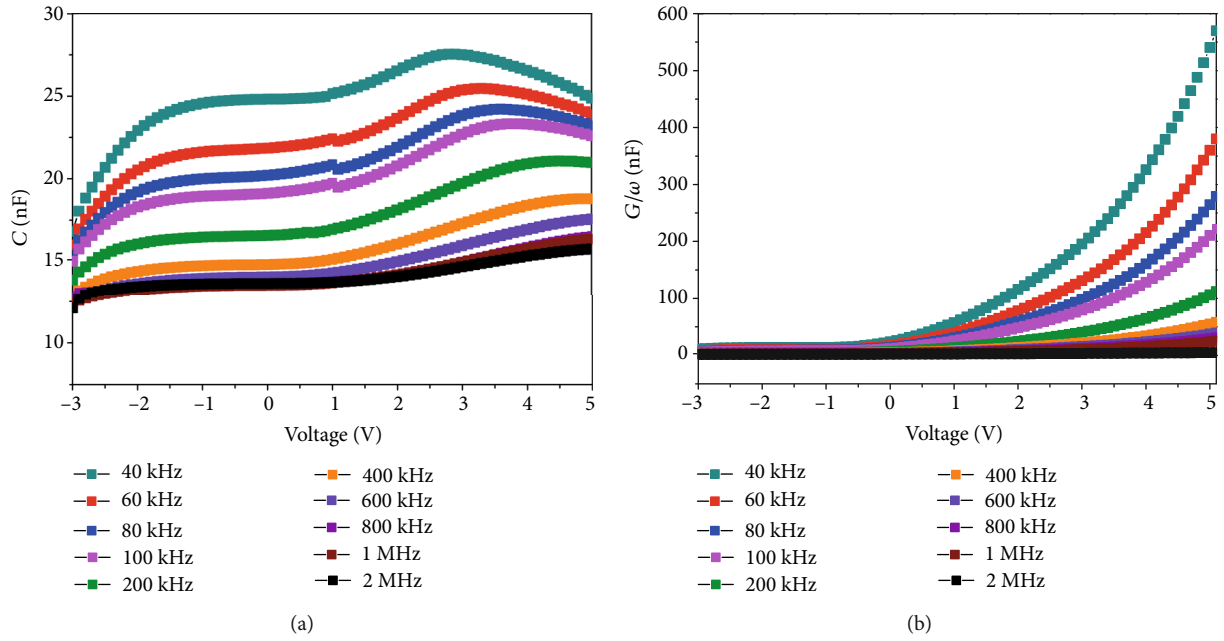

Figure 4: (a) C-V and (b) G/ω-V characteristics of Pd/n-(UNCD/a-C:H:N)/p-Si HJDs.

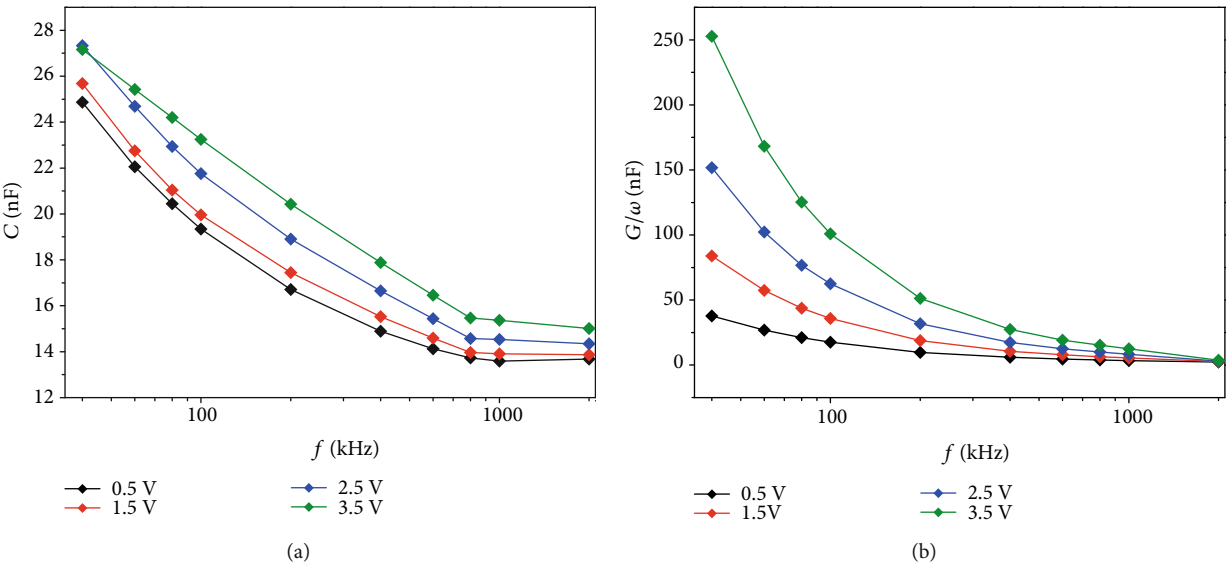

Figure 5: The frequency-dependent (a) C-V and (b) G/ω-V characteristics of Pd/n-(UNCD/a-C:H:N)/p-Si HJDs.

illustrated in Figure 2(b). The suggested mechanism and FTIR results are inconsistent with our previous study [31] which showed the shrinking optical band gap of UNCD/a-C:H films after nitrogen incorporation, due to the increase of the sp^2 fractions.

3.2. Capacitance (C-V-f) and Conductance (G/ω-V-f) Characteristics. It is known that p–n or the Schottky junctions containing deep impurities have significant frequency-dependent capacitance profile [20], and the capacitance vs. frequency relation can determine the characteristics of deep levels in the space-charge region (SCR) of the junction. Figures 4(a) and 4(b) illustrate the C-V and G/ω-V characteristics of Pd/n-(UNCD/a-C:H:N)/p-Si HJD at different frequencies at room temperature. It can be seen that both C and G/ω depend on frequency and bias voltage, which refers to the influence of N_{ss} and R_s [24]. The existence of N_{ss} and R_s can be ascribed to the disruption of the lattice structure at the surface of the fabricated junction as well as the defects on the (UNCD/a-C:H:N)/Si interface [23]. The measured capacitance in Figure 4(a) exhibited a peak in each frequency, shifting to forward bias with increasing frequency until it vanishes at high frequencies. The observed C-V-f curves refer to the existence of different types of interface states, and that the capacitance at low and intermediate frequencies can follow the ac signal but cannot follow at high

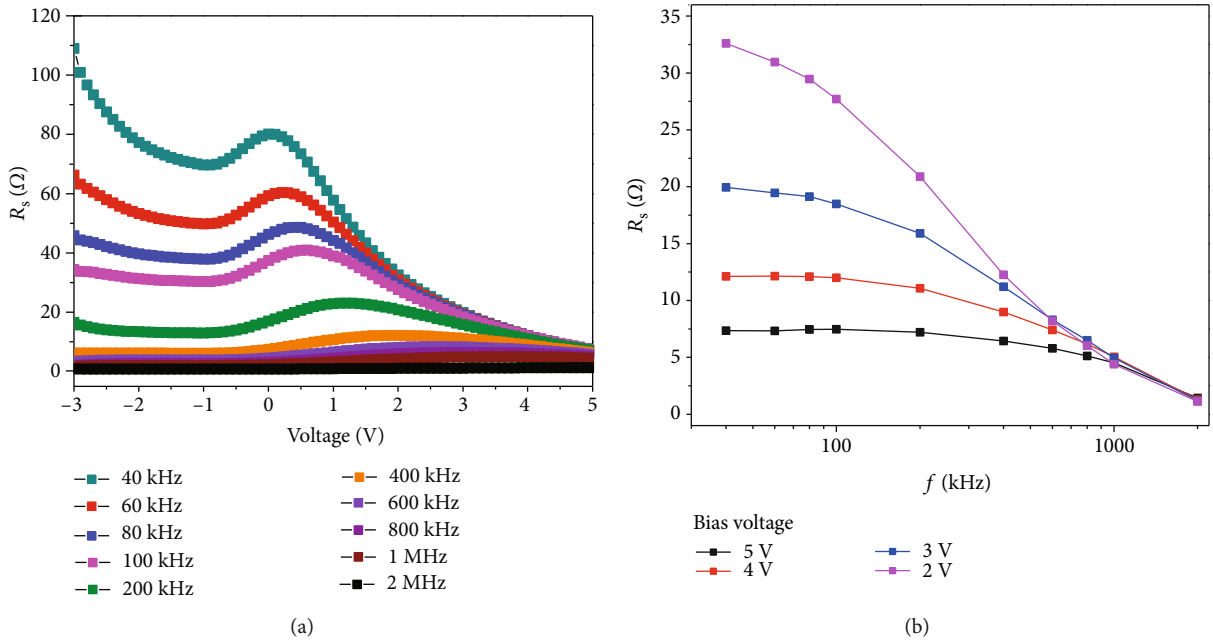

FIGURE 6: R_s as a function of (a) applied bias voltage and (b) frequency at different biases.

frequencies [32]. Almost same trend can be observed for the G/ω-V-f in the depletion region in the same frequency range as displayed in Figure 4(b).

To accurately analyze the influence of ac applied frequencies on the capacitance and conductance profiles, Figures 5(a) and 5(b) illustrate the measured C and G/ω of the Pd/n-(UNCD/a-C:H:N)/p-Si HJD as a function of frequency in the range of 40 kHz to 2 MHz at different voltage biases. As mentioned earlier, C and G/ω are ideally frequency independent, and the deviation from that ideality is mainly due to the existence of N_{ss} and R_s. In Figure 5, both C and G/ω are firmly frequency dependent, especially at low frequencies. The C-V-f profile of the Pd/n-(UNCD/a-C:H:N)/p-Si HJD is consistent with previous studies [33, 34] as follows: at low frequencies, the charges at traps or interface states can follow the ac signal, consequently, and they gain extra capacitance and conductance to the recorded C and G/ω values. On the other hand, at sufficiently higher frequencies, interface states are not capable to follow the ac signal. This behavior is observed for the G/ω-f profile, which indicates the presence of different time-dependent responses of N_{ss}.

3.3. Series Resistance(R_s) and Interface States (N_{ss}) Analysis. Practically, the R_s value of HJDs can be calculated from the capacitance and conductance values at high frequency, by utilizing Nicollian and Goetzberger method [35, 36]:

$$R_s = \frac{G_m}{(\omega C_m)^2 + G_m^2} \quad (1)$$

where C_m and G_m are the measured capacitance and conductance values in the strong accumulation region, respectively. Figure 6(a) showed the biasing voltage dependency of series resistance. R_s exhibits the peaks in the depletion region

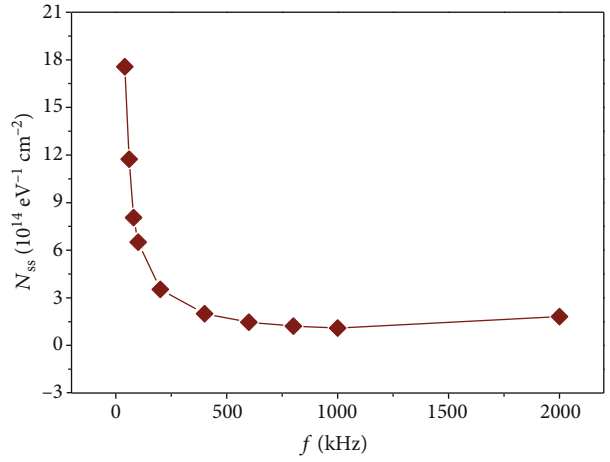

FIGURE 7: N_{ss} vs. frequency for Pd/n-(UNCD/a-C:H:N)/p-Si HJDs.

(-1 V to +1 V) at low frequencies (≤100 kHz), and the peak magnitude decreased from 80 Ω to 40 Ω when the frequency increased from 40 kHz to 100 kHz, respectively. Moreover, the peak decay accompanied by shifted positions towards the accumulation region with increasing frequency. Demirezen et al. [37] explained this observation as a result of reordering and restructuring of carrier charges in the traps under electric field or applied bias voltage. Additionally, Kaya et al. [38] suggested that the voltage-dependent R_s is ascribed to voltage-dependent charges such as interface charge, mobile oxide charge, or oxide-trapped charge. The variation of the series resistance as a function of frequency in the strong accumulation region is plotted in Figure 6(b). It can be seen that R_s has a minimum value at the highest applied frequency (2 MHz). This behavior could be attributed to the distribution density of interface states and their frequency-dependent behavior [23, 39].

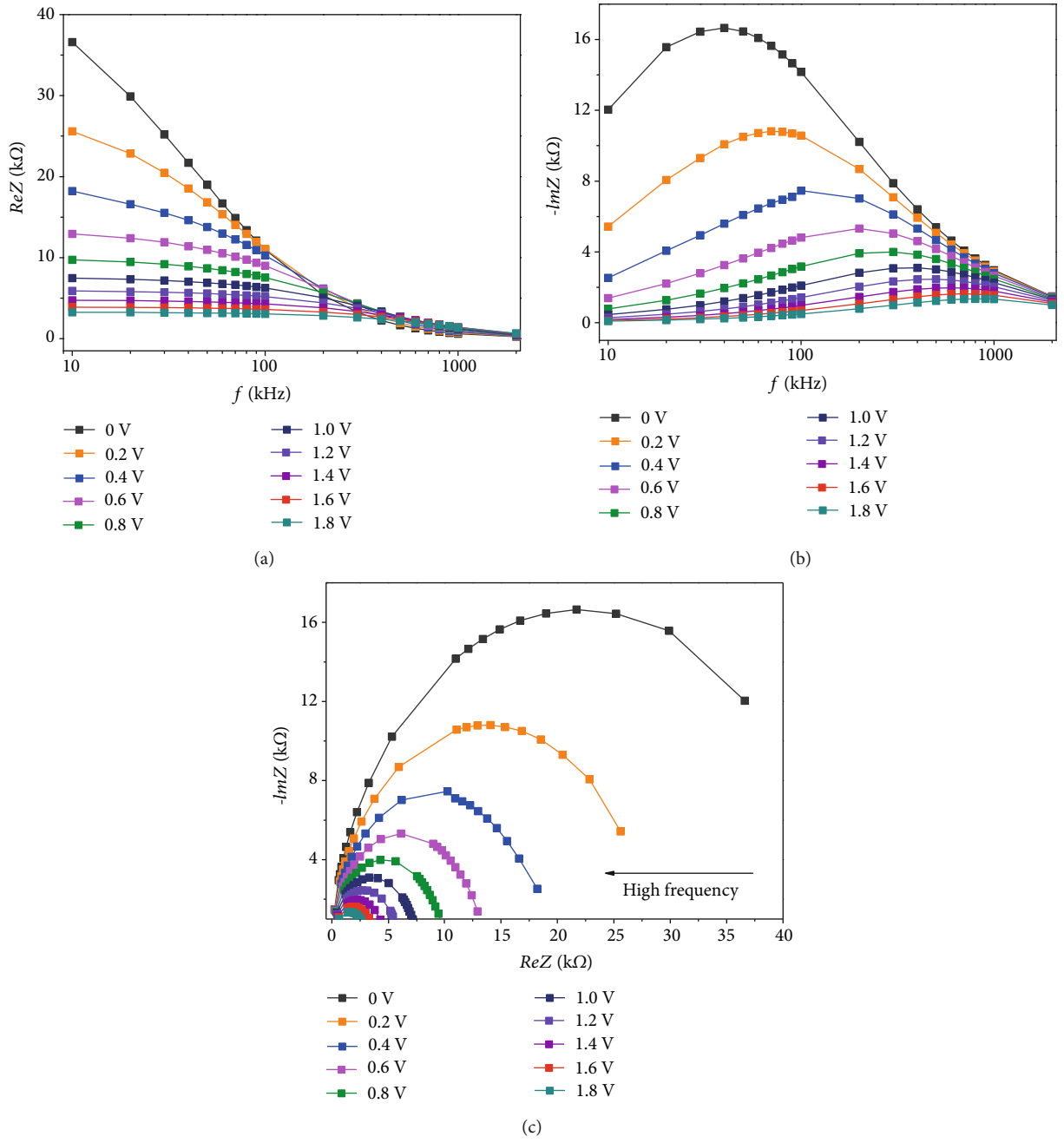

FIGURE 8: (a) *ReZ* and (b) *ImZ* vs. frequency at room temperature. (c) Nyquist impedance spectra of the Pd/*n*-(UNCD/a-C:H:N)/*p*-Si HJD.

Additionally, the Hill-Coleman method is adopted to estimate the N_{ss} values from the measured *C-V* and *G/ω-V*, by equation (2) [18, 40]:

$$N_{ss} = \frac{2}{qA} \frac{(G_{ma}/\omega)_{max}}{\left\{(1 - C_{max}/C_{ox})^2 + \left((G_{ma}/\omega)_{max}/(C_{ox})^2\right\}} \quad (2)$$

Figure 7 represents the frequency dependency of N_{ss} at room temperature. At low and intermediate frequency ranges, N_{ss} has a value of $1.7 \times 10^{15}\,eV^{-1}\,cm^{-2}$ at 40 kHz which decreases rapidly with increasing frequency to the minimum value of $2 \times 10^{14}\,eV^{-1}\,cm^{-2}$ at 400 kHz. Above 500 kHz, the N_{ss} reveals an almost frequency-independent behavior. The calculated N_{ss} values from *C-V* measurements are inconsistent with the values extracted from the experiment and simulation of current-voltage (*I-V*) results previously [16], which indicate a value of defect density of at least $5 \times 10^{17}\,eV^{-1}\,cm^{-3}$ in our Pd/*n*-(UNCD/a-C:H:N)/*p*-Si diode. The results in Figure 7 associate the high value of *C* and *G/ω* at low frequency with the extra capacitance and conductance due to the N_{ss}. In Pd/*n*-(UNCD/a-C:H:N)/*p*-Si

HJD, the interface density can be decreased experimentally by passivation of the UNCD/a-C:H:N layer in the film and at the interface.

3.4. Analysis of the Impedance Spectrum for the Pd/n-(UNCD/a-C:H:N)/p-Si HJD. Impedance spectroscopy is a powerful tool for analyzing the electrical/dielectric properties and for investigating the relaxation process of the electronic devices [41]. It is employed to measure the response of the material to a small amplitude excitation over a range of frequencies (spectrum). Equation (3) describes the complex impedance:

$$Z^* = Z' + iZ'' = ReZ + iImZ, \quad (3)$$

where ReZ is the real part and ImZ is the imaginary part of the complex impedance. Figure 8(a) shows the frequency dependence of real part (ReZ) with the applied ac voltages at the frequency range of 10 Hz to 2 MHz. The ReZ term gradually decreases with increasing applied frequency at the lower frequency, while it revealed a plateau-type behavior at higher frequencies. The results of ReZ can be ascribed to two types of resistance existing in the frequency regions; at low frequency, the resistance is corresponding to recombination resistance(R_{rec}), while at high frequency, it is corresponds to R_s.

The variation of imaginary part of impedance (ImZ) versus the applied frequency is illustrated in Figure 8(b) at different ac voltages. It is observed that the magnitudes of ImZ increase with applied frequency until they reach to a maximum peak (Z_{max}) and then decrease with a further increase of the frequency. It can be seen that the peak of Z_{max} shifts towards the higher frequency region by increasing the applied ac voltages. However, at higher frequency, the curves merge together, which may be caused by accumulation or emergence of space-charge polarization in the Pd/*n*-(UNCD/a-C:H:N)/*p*-Si HJD. This is due to the electrons injected from *n*-UNCD/a-C:H:N layer to space-charge region in *p*-Si side [42].

Impedance spectra of the Pd/*n*-(UNCD/a-C:H:N)/*p*-Si HJD can be obtained from the Cole–Cole plot of the ImZ versus the ReZ in the frequency range of 40 kHz to 2 MHz under different applied AC voltages (from 0 to 1.8 V), as shown in Figure 8(c). The figure depicts a single-semicircle, which indicates a single-carrier device [43]. The radius of the semicircle is related to the total impedance of the device and decreases as the bias increases. The semicircular shape of the impedance spectra in Figure 8(c) indicates that the Pd/*n*-(UNCD/a-C:H:N)/*p*-Si HJD can be represented by an equivalent circuit with a constant phase element (CPE). The CPE impedance (Z_{CPE}) can be given by equation (4) [44]:

$$Z_{CPE} = \frac{1}{\sigma (j\omega)^{\alpha}} \quad (4)$$

where $j = (-1)^{1/2}$, σ represents ac electrical conductivity, and α represents the frequency dependence. Pleskov et al. [45] reported that a CPE (with α close to 1) is a characteristic component of the equivalent circuit of boron-doped diamond.

4. Conclusions

In this study, we have grown nitrogen-doped UNCD/a-C:H:N films by CAPD technique in ambient H2:N2 gaseous mixture. The incorporation of nitrogen into the films have been confirmed by XPS and FTIR measurements. The results indicate the incorporation of nitrogen atoms into the grain boundaries (a-C:H:N) and increase the sp^2 fractions. The constructed heterojunction diodes comprising of the deposited *n*-type (UNCD/a-C:H:N) films onto *p*-type Si substrates were examined by room-temperature *C-V-f* and *G/ω-V-f* in the frequency range of 40 kHz-2 MHz. At low frequencies, the results indicated that the charges at traps could easily follow the ac signal. The bias-dependent profiles R_s exhibited peaks in the depletion region (-1 V to +1 V), which decreased and shifted towards the accumulation region with increasing frequency. This is thought to be due to the restructuring of carrier charges in traps. The high values of C and G/ω were ascribed to the increase in the value of capacitance and conductance that resulted from the N_{ss}, which can follow the ac signal at low frequency, to be almost frequency independent at sufficient high-applied frequencies. Results of frequency-dependent impedance spectroscopy exhibited a plateau-type behavior at high frequencies, corresponding to the series resistance. These results show that nitrogen-doped *n*-type (UNCD/a-C:H:N) thin films are applicable semiconductors in diamond-based electronic devices.

Data Availability

The data used to support the findings of this study are available from the corresponding authors upon request.

Conflicts of Interest

The authors declare that they have no conflicts of interest.

Acknowledgments

A. Zkria acknowledges the Japan Society for Promotion of Science (JSPS) for awarding the JSPS fellowship-standard. This work was supported by the Advanced Low Carbon Technology Research and Development Program (ALCA) of the Japan Science and Technology Agency (JST) JSPS KAKENHI (Grant No. JP15H04127 and JP16K18238) and Grant-in-Aid for JSPS Fellows (Grant No. JP17F17380).

References

[1] S. Koizumi, H. Umezawa, J. Pernot, and M. Suzuki, *Power electronics device applications of diamond semiconductors*, Woodhead Publishing, United Kingdom, 2018.

[2] Y. J. Lu, C. N. Lin, and C. X. Shan, "Optoelectronic diamond: growth, properties, and photodetection applications," *Advanced Optical Materials*, vol. 6, no. 20, p. 1800359, 2018.

[3] E. Rohrer, C. F. O. Graeff, R. Janssen et al., "Nitrogen-related dopant and defect states in CVD diamond," *Physical Review B*, vol. 54, no. 11, pp. 7874–7880, 1996.

[4] O. A. Williams, S. Curat, J. E. Gerbi, D. M. Gruen, and R. B. Jackman, "n-type conductivity in ultrananocrystalline

diamond films," *Applied Physics Letters*, vol. 85, no. 10, pp. 1680–1682, 2004.

[5] J. Birrell, J. E. Gerbi, O. Auciello, J. M. Gibson, D. M. Gruen, and J. A. Carlisle, "Bonding structure in nitrogen doped ultrananocrystalline diamond," *Journal of Applied Physics*, vol. 93, no. 9, pp. 5606–5612, 2003.

[6] T. Ikeda, K. Teii, C. Casiraghi, J. Robertson, and A. C. Ferrari, "Effect of the sp[sup 2] carbon phase on n-type conduction in nanodiamond films," *Journal of Applied Physics*, vol. 104, no. 7, article 073720, 2008.

[7] M. Mertens, M. Mohr, N. Wiora, K. Bruehne, and H.-J. Fecht, "N-Type Conductive Ultrananocrystalline Diamond Films Grown by Hot Filament CVD," *Journal of Nanomaterials*, vol. 2015, Article ID 527025, 6 pages, 2015.

[8] C. Popov, W. Kulisch, M. Jelinek, A. Bock, and J. Strnad, "Nanocrystalline diamond/amorphous carbon composite films for applications in tribology, optics and biomedicine," *Thin Solid Films*, vol. 494, no. 1-2, pp. 92–97, 2006.

[9] D. M. Gruen, "Nanocrystalline diamond films," *Annual Review of Materials Science*, vol. 29, no. 1, pp. 211–259, 1999.

[10] A. Zkria, F. Abdel-Wahab, Y. Katamune, and T. Yoshitake, "Optical and structural characterization of ultrananocrystalline diamond/hydrogenated amorphous carbon composite films deposited via coaxial arc plasma," *Current Applied Physics*, vol. 19, no. 2, pp. 143–148, 2019.

[11] S. Al-Riyami, S. Ohmagari, and T. Yoshitake, "Nitrogen-doped ultrananocrystalline diamond/hydrogenated amorphous carbon composite films prepared by pulsed laser deposition," *Applied Physics Express*, vol. 3, no. 11, p. 115102, 2010.

[12] A. Zkria, H. Gima, M. Shaban, and T. Yoshitake, "Electrical characteristics of nitrogen-doped ultrananocrystalline diamond/hydrogenated amorphous carbon composite films prepared by coaxial arc plasma deposition," *Applied Physics Express*, vol. 8, no. 9, article 095101, 2015.

[13] A. Zkria, M. Shaban, T. Hanada, N. Promros, and T. Yoshitake, "Current transport mechanisms in n-type ultrananocrystalline diamond/p-type Si heterojunctions," *Journal of Nanoscience and Nanotechnology*, vol. 16, no. 12, pp. 12749–12753, 2016.

[14] A. Zkria, H. Gima, and T. Yoshitake, "Application of nitrogen-doped ultrananocrystalline diamond/hydrogenated amorphous carbon composite films for ultraviolet detection," *Applied Physics A*, vol. 123, no. 3, 2017.

[15] A. Zkria and T. Yoshitake, "Temperature-dependent current–voltage characteristics and ultraviolet light detection of heterojunction diodes comprising n-type ultrananocrystalline diamond/hydrogenated amorphous carbon composite films and p-type silicon substrates," *Japanese Journal of Applied Physics*, vol. 56, no. 7S2, p. 07KD04, 2017.

[16] M. Shaban, A. Zkria, and T. Yoshitake, "Characterization and design optimization of heterojunction photodiodes comprising n-type ultrananocrystalline diamond/hydrogenated amorphous carbon composite and p-type Si," *Materials Science in Semiconductor Processing*, vol. 86, pp. 115–121, 2018.

[17] E. H. Nicollian, *MOS (Metal Oxide Semiconductor) Physics and Technology*, Wiley-Interscience, New Jersey, USA, 2002.

[18] W. Hill and C. Coleman, "A single-frequency approximation for interface-state density determination," *Solid State Electronics*, vol. 23, no. 9, pp. 987–993, 1980.

[19] N. C. Saha and M. Kasu, "Heterointerface properties of diamond MOS structures studied using capacitance–voltage and conductance–frequency measurements," *Diamond and Related Materials*, vol. 91, pp. 219–224, 2019.

[20] S. A. Yerişkin, M. Balbaşı, and İ. Orak, "Frequency dependent electrical characteristics and origin of anomalous capacitance–voltage (C–V) peak in Au/(graphene-doped PVA)/n-Si capacitors," *Journal of Materials Science: Materials in Electronics*, vol. 28, no. 11, pp. 7819–7826, 2017.

[21] I. S. Yahia, M. Fadel, G. B. Sakr, S. S. Shenouda, and F. Yakuphanoglu, "Effect of the frequency and temperature on the complex impedance spectroscopy (C–V and G–V) of p-ZnGa2Se4/n-Si nanostructure heterojunction diode," *Journal of Materials Science*, vol. 47, no. 4, pp. 1719–1728, 2012.

[22] S. S. Fouad, G. B. Sakr, I. S. Yahia, D. M. Abdel-Basset, and F. Yakuphanoglu, "Impedance spectroscopy of p-ZnGa2-Te4/n-Si nano-HJD," *Physica B*, vol. 415, pp. 82–91, 2013.

[23] B. Akkal, Z. Benamara, B. Gruzza, and L. Bideux, "Characterization of interface states at Au/InSb/InP(100) Schottky barrier diodes as a function of frequency," *Vacuum*, vol. 57, no. 2, pp. 219–228, 2000.

[24] F. Z. Acar, A. Buyukbas-Ulusan, and A. Tataroglu, "Analysis of interface states in Au/ZnO/p-InP (MOS) structure," *Journal of Materials Science: Materials in Electronics*, vol. 29, no. 15, pp. 12553–12560, 2018.

[25] H. Gima, A. Zkria, Y. Katamune, R. Ohtani, S. Koizumi, and T. Yoshitake, "Chemical bonding structural analysis of nitrogen-doped ultrananocrystalline diamond/hydrogenated amorphous carbon composite films prepared by coaxial arc plasma deposition," *Applied Physics Express*, vol. 10, no. 1, article 015801, 2017.

[26] M. Cardona and L. Ley, *Photoemission in Solids I, General Principles*, Springer, Verlag, Berlin, Heidelberg, New York, 1978.

[27] R. McCann, S. S. Roy, P. Papakonstantinou, M. F. Bain, H. S. Gamble, and J. A. Mclaughlin, "Chemical bonding modifications of tetrahedral amorphous carbon and nitrogenated tetrahedral amorphous carbon films induced by rapid thermal annealing," *Thin Solid Films*, vol. 482, no. 1-2, pp. 34–40, 2005.

[28] T. Yoshitake, A. Nagano, S. Ohmagari et al., "Near-edge X-ray absorption fine-structure, X-ray photoemission, and Fourier transform infrared spectroscopies of ultrananocrystalline diamond/hydrogenated amorphous carbon composite films," *Japanese Journal of Applied Physics*, vol. 48, no. 2, article 020222, 2009.

[29] C. J. Tang, M. A. Neto, M. J. Soares, A. J. S. Fernandes, A. J. Neves, and J. Gráciob, "A comparison study of hydrogen incorporation among nanocrystalline, microcrystalline and polycrystalline diamond films grown by chemical vapor deposition," *Thin Solid Films*, vol. 515, no. 7-8, pp. 3539–3546, 2007.

[30] S. Xuguang, "The investigation of chemical structure of coal macerals via transmitted-light FT-IR microspectroscopy," *Spectrochimica Acta Part A: Molecular and Biomolecular Spectroscopy*, vol. 62, no. 1-3, pp. 557–564, 2005.

[31] A. Zkria, Y. Katamune, and T. Yoshitake, "Effects of nitrogen doping on the electrical conductivity and optical absorption of ultrananocrystalline diamond/hydrogenated amorphous carbon films prepared by coaxial arc plasma deposition," *Japanese Journal of Applied Physics*, vol. 55, no. 7S2, article 07LE01, 2016.

[32] A. Buyukbas-Uluşan, S. Altındal Yerişkin, A. Tataroğlu, M. Balbaşı, and Y. Azizian Kalandaragh, "Electrical and impedance properties of MPS structure based on (Cu2O–

CuO–PVA) interfacial layer," *Journal of Materials Science: Materials in Electronics*, vol. 29, no. 10, p. 8234, 2018.

[33] V. N. Reddy, R. Padma, and K. R. Gunasekhar, "Analysis of electronic parameters and frequency-dependent properties of Au/NiO/n-GaN heterojunctions," *Applied Physics A*, vol. 124, no. 1, p. 1, 2018.

[34] Ç. Bilkan, Ş. Altındal, and Y. Azizian-Kalandaragh, "Investigation of frequency and voltage dependence surface states and series resistance profiles using admittance measurements in Al/p-Si with Co 3 O 4 -PVA interlayer structures," *Physica B: Condensed Matter*, vol. 515, pp. 28–33, 2017.

[35] E. H. Nicollian and A. Goetzberger, "MOS conductance technique for measuring surface state parameters," *Applied Physics Letters*, vol. 7, no. 8, pp. 216–219, 1965.

[36] E. H. Nicollian and A. Goetzberger, "The Si-SiO2 interface - electrical properties as determined by the metal-insulator-silicon conductance technique," *Bell System Technical Journal*, vol. 46, no. 6, pp. 1055–1133, 1967.

[37] S. Demirezen, Z. Sönmez, U. Aydemir, and Ş. Altındal, "Effect of series resistance and interface states on the I–V, C–V and G/ω–V characteristics in Au/Bi-doped polyvinyl alcohol (PVA)/n-Si Schottky barrier diodes at room temperature," *Current Applied Physics*, vol. 12, no. 1, pp. 266–272, 2012.

[38] S. Kaya, R. Lok, A. Aktag, J. Seidel, and E. Yilmaz, "Frequency dependent electrical characteristics of $BiFeO_3$ MOS capacitors," *Journal of Alloys and Compounds*, vol. 583, pp. 476–480, 2014.

[39] A. A. M. Farag, B. Gunduz, F. Yakuphanoglu, and W. A. Farooq, "Controlling of electrical characteristics of Al/p-Si Schottky diode by tris(8-hydroxyquinolinato) aluminum organic film," *Synthetic Metals*, vol. 160, no. 23-24, pp. 2559–2563, 2010.

[40] Ç. Bilkan and Ş. Altındal, "Investigation of the C-V characteristics that provides linearity in a large reverse bias region and the effects of series resistance, surface states and interlayer in Au/n-Si/Ag diodes," *Journal of Alloys and Compounds*, vol. 708, pp. 464–469, 2017.

[41] A. Buyukbas-Ulusan, İ. Taşçıoğlu, A. Tataroğlu, F. Yakuphanoğlu, and S. Altındal, "A comparative study on the electrical and dielectric properties of Al/Cd-doped ZnO/p-Si structures," *Journal of Materials Science: Materials in Electronics*, vol. 30, no. 13, pp. 12122–12129, 2019.

[42] L. Singh, I. W. Kim, W. S. Woo, B. C. Sin, H. I. Lee, and Y. Lee, "A novel low cost non-aqueous chemical route for giant dielectric constant CaCu3Ti4O12 ceramic," *Solid State Sciences*, vol. 43, pp. 35–45, 2015.

[43] C. Jonda and A. B. R. Mayer, "Investigation of the electronic properties of organic light-emitting devices by impedance spectroscopy," *Chemistry of Materials*, vol. 11, no. 9, pp. 2429–2435, 1999.

[44] J. R. Macdonald and W. B. Johnson, *Impedance Spectroscopy*, J. R. Macdonald, Ed., Wiley, New York, 1987.

[45] Y. V. Pleskov, V. Ya, M. A. A. Mishuk et al., "Synthetic semiconductor diamond electrodes: determination of acceptor concentration by linear and non-linear impedance measurements," *Journal of Electroanalytical Chemistry*, vol. 396, no. 1-2, pp. 227–232, 1995.